Magnetohydrodynamic Thermal Rotating Shallow Water Systems

Yangyang Cao[1], Alexander Kurganov[2,6], Masoud Rostami[3,4,6], Chenxi Wang[5,6], and Vladimir Zeitlin[6]

[1]MSU-BIT-SMBU Joint Research Center of Applied Mathematics, Shenzhen MSU-BIT University, Shenzhen 518172, China

[2]Department of Mathematics, Southern University of Science and Technology (SUSTech), Shenzhen 518055, China

[3]Potsdam Institute for Climate Impact Research (PIK), Member of the Leibniz Association, Potsdam, Germany

[4]Laboratoire de Météorologie Dynamique (LMD) / IPSL, ENS-PSL Université, Ecole Polytechnique-Institut Polytechnique de Paris, Sorbonne Université,, CNRS, Paris, France

[5]School of Science, Harbin Institute of Technology, Shenzhen 518055, China

[6]Shenzhen International Center for Mathematics, Southern University of Science and Technology (SUSTech), Shenzhen 518055, China

This is the Authors Original Manuscript (AOM); that is, the manuscript in its original form; a preprint . The Version of Record of this manuscript has been published and is available in the: "Physical Review Fluids": https://doi.org/10.1103/cbq8-4wmc

How to cite:

Cao, Y., Kurganov, A., Rostami, M., Wang, C., & Zeitlin, V. (2026). Magnetohydrodynamic thermal rotating shallow water systems. *Physical Review Fluids*, **11**, L011701. https://doi.org/10.1103/cbq8-4wmc

Magnetohydrodynamic Thermal Rotating Shallow Water Systems

[a]Yangyang Cao[1], Alexander Kurganov[2,6], Masoud Rostami[b,3,4,6], Chenxi Wang[5,6], and Vladimir Zeitlin[4]

[1]*MSU-BIT-SMBU Joint Research Center of Applied Mathematics, Shenzhen MSU-BIT University, Shenzhen, 518172, China*
[2]*Department of Mathematics, Southern University of Science and Technology, Shenzhen 518055, China*
[3]*Potsdam Institute for Climate Impact Research (PIK), Member of the Leibniz Association, Potsdam, Germany*
[4]*Laboratoire de Météorologie Dynamique (LMD) / IPSL, ENS-PSL Université, Ecole Polytechnique-Institut Polytechnique de Paris, Sorbonne Université, CNRS, Paris, France*
[5]*School of Science, Harbin Institute of Technology, Shenzhen 518055, China*
[6]*Shenzhen International Center for Mathematics, Southern University of Science and Technology, Shenzhen, 518055, China*

ABSTRACT

We introduce the *Magnetohydrodynamic Thermal Rotating Shallow Water (MTRSW)* model as a framework to study magnetized rotating fluids influenced by thermal gradients and stratification. The model is derived from the full magnetohydrodynamic equations incorporating Coriolis forces, magnetic induction, and thermal effects. To extend its applicability to small-scale magnetic dynamics, Hall MTRSW corrections are included. The proposed MTRSW systems are particularly applicable for thin, magnetized, rotating stratified layers, such as the solar tachocline, neutron star oceans, and accretion disks with shallow vertical extent. Numerical simulations confirm that thermal and magnetic coupling substantially impacts the stability and evolution of vortices, with nontrivial temperature gradients fostering prolonged instabilities.

The main objective of this study is to introduce a magnetohydrodynamic thermal rotating shallow water (MTRSW) equations. The new model is systematically derived from the full magnetohydrodynamic (MHD) equations using vertical averaging techniques, while delineating the fundamental assumptions underlying its formulation. Unlike classical rotating shallow water (RSW) models, thermal rotating shallow water (TRSW) models introduce inhomogeneous layers, allowing for horizontal variations in material properties. This characteristic has earned them the alternative name *inhomogeneous-layer models* in the literature [7, 8].

The shallow water MHD framework, which serves as a precursor to this study, was first introduced by Gilman [2] to model the solar tachocline, where the mean density of the fluid is assumed to be constant. In contrast, this study incorporates density variations that, in an atmospheric context, correspond to changes in (potential) temperature.

The TRSW framework, grounded in a robust theoretical foundation, has been widely applied to investigate phenomena such as the dynamics of a well-mixed planetary boundary layer [6] and reduced two-dimensional models of deep atmospheric motions under simple stratification [12]. Recent advances [3–5, 10, 11] further underscore its versatility and significance in exploring diverse physical processes. In particular, the TRSW model has recently been implemented as the dynamical core of an intermediate complexity atmospheric model, Aeolus 2.0 [11].

The MTRSW model developed in this work advances the treatment of ion-scale physics through systematic incorporation of the Hall term in the governing equations. This implementation introduces scale-dependent dynamics via the Hall current, a critical feature absent in conventional MHD. The Hall-MTRSW framework captures three fundamental small-scale phenomena. First, it enables fast magnetic reconnection through breakdown of the frozen-in condition at ion-inertial scales, allowing topological restructuring of magnetic field lines. Second, it modifies Alfvén wave propagation characteristics through dispersion relations that now incorporate ion-scale physics. Third, it naturally accounts for ion-electron decoupling effects inherent in Hall-MHD systems. Together, these capabilities provide a unified description of multi-scale plasma dynamics in rotating, thermally stratified environments.

The core contribution of this study lies in the first-principles derivation of the governing equations for the MTRSW model, including both standard and Hall-effect terms. A comprehensive validation of the numerical scheme and extended model applications are provided in a separate companion study [1].

As a starting point, we consider the inviscid incompressible three-dimensional (3D) MHD equations to describe the dynamics of a conducting fluid with variable density. The governing equations include fluid motion, magnetic field evolution, and the divergence-free constraints on both the velocity and magnetic flux. These equations are expressed as follows:

$$\rho\left(\partial_t \boldsymbol{v} + \boldsymbol{v}\cdot\nabla\boldsymbol{v} + f\boldsymbol{z}\times\boldsymbol{v}\right) = -\rho g\boldsymbol{z} - \nabla p + \boldsymbol{F}_L, \tag{1}$$

$$\partial_t \rho + \nabla\cdot(\rho\boldsymbol{v}) = 0, \tag{2}$$

$$\partial_t \boldsymbol{B} = \nabla\times(\boldsymbol{v}\times\boldsymbol{B}), \tag{3}$$

$$\nabla\cdot\boldsymbol{B} = 0, \quad \nabla\cdot\boldsymbol{v} = 0. \tag{4}$$

Here, $\boldsymbol{v} = (u,v,w)^\top$ represents the 3D velocity field, where the $(\cdot)^\top$ denotes the transpose operation, ρ is the fluid density, and p denotes the pressure. The Coriolis term $f = 2\Omega$ accounts for the rotation of the planet, with Ω being the angular velocity and $\boldsymbol{z}$ being

[a] Author list in alphabetical order.
[b] Author to whom correspondence should be addressed: rostamimasoud@yahoo.com or rostami@lmd.ipsl.fr

the vertical unit vector. The effective gravitational acceleration is represented as $-g\boldsymbol{z}$. The operator $\nabla = (\partial_x, \partial_y, \partial_z)^\top$ represents the 3D gradient. The Lorentz force, $\boldsymbol{F}_L = \boldsymbol{J} \times \boldsymbol{B}$, arises from the interaction between the magnetic field, $\boldsymbol{B} = (a,b,c)^\top$, and the current density, $\boldsymbol{J}$. Using Ampère's law, $\boldsymbol{J} = \frac{1}{\mu_0}(\nabla \times \boldsymbol{B})$, where μ_0 is the magnetic permeability of free space, the Lorentz force in equation (1) becomes

$$\boldsymbol{F}_L = \frac{1}{\mu_0}(\nabla \times \boldsymbol{B}) \times \boldsymbol{B} = \frac{1}{\mu_0}\Big[(\boldsymbol{B}\cdot\nabla)\boldsymbol{B} - \frac{1}{2}\nabla|\boldsymbol{B}|^2\Big]. \tag{5}$$

Here, the term $(\boldsymbol{B}\cdot\nabla)\boldsymbol{B}$ represents the magnetic tension force, which acts as a restoring force directed radially inward with respect to magnetic field line curvature, while $\frac{1}{2}\nabla|\boldsymbol{B}|^2$ represents the magnetic pressure gradient force, acting perpendicular to the field lines. The pressure gradient term, $-\nabla p$, drives fluid motion by directing it from regions of high pressure to low pressure. The continuity equation (2) governs the conservation of mass. The evolution of the magnetic field is governed by the induction equation (3). For applications requiring magnetic reconnection, resistive effects can be incorporated by adding the diffusion term $\eta\nabla^2\boldsymbol{B}$ to the induction equation, where η is the magnetic diffusivity. Expanding the first term on the right-hand side (RHS) of (3) yields

$$\nabla \times (\boldsymbol{v} \times \boldsymbol{B}) = \nabla\cdot(\boldsymbol{B}\otimes\boldsymbol{v}) - \nabla\cdot(\boldsymbol{v}\otimes\boldsymbol{B}), \tag{6}$$

where each term represents distinct physical processes. The term $\nabla\cdot(\boldsymbol{B}\otimes\boldsymbol{v})$ describes the stretching of the velocity gradient along the magnetic field lines, while $-\nabla\cdot(\boldsymbol{v}\otimes\boldsymbol{B})$ accounts for the advection of the magnetic field by the fluid flow. We note that in equation (6), as well as in the other equations presented in this paper, the shorthand notation $\nabla\cdot(A\otimes B) := \partial_j(A_jB_k)$, $j,k = 1,2,3$, is used to denote the divergence of the tensor product of the vector fields A and B.

When the effects of viscosity and magnetic diffusion are negligible, the momentum equation (1) and the magnetic field evolution (3) can be reformulated as conservation laws. This reformulation utilizes equations (2) and (5) and absorbs the magnetic permeability (μ_0) into the magnetic field $\boldsymbol{B}$ by replacing $\frac{1}{\sqrt{\mu_0}}\boldsymbol{B}$ with $\boldsymbol{B}$, resulting in the following conservative form:

$$\partial_t(\rho\boldsymbol{v}) + \nabla\cdot(\rho\boldsymbol{v}\otimes\boldsymbol{v}) + f\boldsymbol{z}\times(\rho\boldsymbol{v}) = -\rho g\boldsymbol{z} - \nabla p^* + \nabla\cdot(\boldsymbol{B}\otimes\boldsymbol{B}), \tag{7}$$
$$\partial_t\boldsymbol{B} = \nabla\cdot(\boldsymbol{B}\otimes\boldsymbol{v}) - \nabla\cdot(\boldsymbol{v}\otimes\boldsymbol{B}). \tag{8}$$

Here, p^* represents the modified geopotential, defined as $p^* := p + \frac{1}{2}|\boldsymbol{B}|^2$. Thus, p^* combines the effects of both fluid pressure and magnetic pressure into a single scalar quantity.

We now vertically integrate equations (2), (4), (7), and (8), between two material surfaces $z_{i-1}(x,y,t)$ and $z_i(x,y,t)$, $i = 1,2,3,\ldots$, which are defined to move with the local vertical velocity of the fluid w and are simultaneously assumed to act as magnetic surfaces, that is, all z_i satisfy

$$w\big|_{z_i} = \partial_t z_i + u\partial_x z_i + v\partial_y z_i, \tag{9}$$
$$\boldsymbol{B}\cdot\nabla(z - z_i) = 0. \tag{10}$$

By applying the Leibniz rule for moving boundaries, which for a generic quantity $Q(x,y,z,t)$ integrated between material surfaces $z_{i-1}(x,y,t)$ and $z_i(x,y,t)$ states: $\frac{\partial}{\partial t}\int_{z_{i-1}}^{z_i} Q\,dz = \int_{z_{i-1}}^{z_i}\frac{\partial Q}{\partial t}\,dz + Q|_{z_i}\frac{\partial z_i}{\partial t} - Q|_{z_{i-1}}\frac{\partial z_{i-1}}{\partial t}$, and taking into account (9) and (10), we obtain

$$\begin{aligned}\partial_t\int_{z_{i-1}}^{z_i}(\rho\boldsymbol{v}_h)\,\mathrm{d}z + \nabla_h\cdot\int_{z_{i-1}}^{z_i}(\rho\boldsymbol{v}_h\otimes\boldsymbol{v}_h)\,\mathrm{d}z + f\boldsymbol{z}\times\int_{z_{i-1}}^{z_i}(\rho\boldsymbol{v}_h)\,\mathrm{d}z = \\ -\nabla_h\int_{z_{i-1}}^{z_i}p^*\,\mathrm{d}z + \nabla_h z_i\,p^*\big|_{z_i} - \nabla_h z_{i-1}\,p^*\big|_{z_{i-1}} + \nabla_h\cdot\int_{z_{i-1}}^{z_i}(\boldsymbol{B}_h\otimes\boldsymbol{B}_h)\,\mathrm{d}z,\end{aligned} \tag{11}$$
$$\partial_t\int_{z_{i-1}}^{z_i}\rho\,\mathrm{d}z + \nabla_h\cdot\int_{z_{i-1}}^{z_i}(\rho\boldsymbol{v}_h)\,\mathrm{d}z = 0, \tag{12}$$
$$\partial_t\int_{z_{i-1}}^{z_i}\boldsymbol{B}_h\,\mathrm{d}z = \nabla_h\cdot\int_{z_{i-1}}^{z_i}(\boldsymbol{B}_h\otimes\boldsymbol{v}_h)\,\mathrm{d}z - \nabla_h\cdot\int_{z_{i-1}}^{z_i}(\boldsymbol{v}_h\otimes\boldsymbol{B}_h)\,\mathrm{d}z, \tag{13}$$
$$\nabla_h\cdot\int_{z_{i-1}}^{z_i}\boldsymbol{B}_h\,\mathrm{d}z = 0, \quad \partial_t(z_i - z_{i-1}) + \nabla_h\cdot\int_{z_{i-1}}^{z_i}\boldsymbol{v}_h\,\mathrm{d}z = 0, \tag{14}$$

where $\nabla_h := (\partial_x,\partial_y)^\top$, $\boldsymbol{v}_h := (u,v)^\top$, and $\boldsymbol{B}_h := (a,b)^\top$ are horizontal components of ∇, $\boldsymbol{v}$, and $\boldsymbol{B}$, respectively. Notice that in (11)–(14), we have ignored the equations for ρw and c as they are getting decoupled from the other equations. Once the other fields are determined, both w and c can be recovered from (4):

$$w(x,y,z,t) = w(x,y,t)\big|_{z_{i-1}} - (z-z_{i-1})\nabla_h \cdot \boldsymbol{v}_h, \tag{15}$$

$$c(x,y,z,t) = c(x,y,t)\big|_{z_{i-1}} - (z-z_{i-1})\nabla_h \cdot \boldsymbol{B}_h, \tag{16}$$

where $z_{i-1} < z < z_i$. Equation (15) is derived by vertically integrating the incompressibility condition $\nabla \cdot \boldsymbol{v} = 0$ from the lower boundary z_{i-1} to an arbitrary height z, using the horizontal divergence $\nabla_h \cdot \boldsymbol{v}_h$. Similarly, Eq. (16) results from integrating the solenoidal constraint $\nabla \cdot \boldsymbol{B} = 0$. We now introduce the following notation. For the quantities A and B, their averages will be denoted by $\overline{A}_i := \frac{1}{z_i - z_{i-1}} \int_{z_{i-1}}^{z_i} A \, \mathrm{d}z$ and $\overline{B}_i := \frac{1}{z_i - z_{i-1}} \int_{z_{i-1}}^{z_i} B \, \mathrm{d}z$, and we then use the mean-field approximation $\overline{A_i B_i} \approx \overline{A}_i \cdot \overline{B}_i$ to obtain the following averaged version of (11)–(14):

$$\begin{aligned}
&\overline{\rho}_i (z_i - z_{i-1}) \left(\partial_t \overline{\boldsymbol{v}}_{h,i} + \overline{\boldsymbol{v}}_{h,i} \cdot \nabla_h \overline{\boldsymbol{v}}_{h,i} + f \boldsymbol{z} \times \overline{\boldsymbol{v}}_{h,i} \right) = \\
&\qquad - \nabla_h \int_{z_{i-1}}^{z_i} p^* \, \mathrm{d}z + \nabla_h z_i \, p^*\big|_{z_i} - \nabla_h z_{i-1} \, p^*\big|_{z_{i-1}} + \nabla_h \cdot \left[(z_i - z_{i-1}) \overline{\boldsymbol{B}}_{h,i} \otimes \overline{\boldsymbol{B}}_{h,i} \right], \qquad (17) \\
&\partial_t \left[\overline{\rho}_i (z_i - z_{i-1}) \right] + \nabla_h \cdot \left[\overline{\rho}_i (z_i - z_{i-1}) \overline{\boldsymbol{v}}_{h,i} \right] = 0, \qquad (18) \\
&\partial_t \left[(z_i - z_{i-1}) \overline{\boldsymbol{B}}_{h,i} \right] = \nabla_h \cdot \left[(z_i - z_{i-1}) \overline{\boldsymbol{B}}_{h,i} \otimes \overline{\boldsymbol{v}}_{h,i} \right] - \nabla_h \cdot \left[(z_i - z_{i-1}) \overline{\boldsymbol{v}}_{h,i} \otimes \overline{\boldsymbol{B}}_{h,i} \right], \qquad (19) \\
&\nabla_h \cdot \left[(z_i - z_{i-1}) \overline{\boldsymbol{B}}_{h,i} \right] = 0, \quad \partial_t (z_i - z_{i-1}) + \nabla_h \cdot \left[(z_i - z_{i-1}) \overline{\boldsymbol{v}}_{h,i} \right] = 0. \qquad (20)
\end{aligned}$$

Remark .1 *It is important to note that corrections to the mean-field approximation can be incorporated, when necessary, through the application of turbulent viscosity and diffusivity parameterizations. The mean-field equations contain gradients of generalized Reynolds stresses, which represent the influence of unresolved subgrid-scale motions on the mean flow. While standard eddy diffusivity closures model these terms as being proportional to the gradients of the corresponding mean fields, more sophisticated parameterizations accounting for non-diffusive momentum and magnetic flux transport could be implemented for turbulent regimes. Such closures would introduce additional terms beyond simple Laplacian diffusion in both the averaged momentum and magnetic evolution equations.*

To derive the MTRSW equations from the vertically averaged MHD system (17)–(20), we introduce the *magnetohydrostatic balance hypothesis*, which assumes that vertical accelerations are negligible:

$$\partial_z p^* = -\rho g. \tag{21}$$

By integrating (21) with respect to z, the modified pressure $p^*\big|_z$ is obtained as

$$p^*\big|_z \approx -\overline{\rho}_i g (z - z_{i-1}) + p^*\big|_{z_{i-1}}, \tag{22}$$

which can now be integrated over the layer $z_{i-1} < z < z_i$ to yield

$$\int_{z_{i-1}}^{z_i} p^* \, \mathrm{d}z \approx -\frac{1}{2} \overline{\rho}_i g (z_i - z_{i-1})^2 + (z_i - z_{i-1}) \, p^*\big|_{z_{i-1}}. \tag{23}$$

Substituting (23) into (17) results in the following *master equation* for the MTRSW model, which is valid within the layer bounded by the material surfaces:

$$\begin{aligned}
\overline{\rho}_i h_i \left(\partial_t \overline{\boldsymbol{v}}_{h,i} + \overline{\boldsymbol{v}}_{h,i} \cdot \nabla_h \overline{\boldsymbol{v}}_{h,i} + f \boldsymbol{z} \times \overline{\boldsymbol{v}}_{h,i} \right) = &- \nabla_h \Big(- \frac{1}{2} \overline{\rho}_i g h_i^2 + h_i p^*\big|_{z_{i-1}} \Big) \\
&+ \nabla_h z_i \, p^*\big|_{z_i} - \nabla_h z_{i-1} \, p^*\big|_{z_{i-1}} + \nabla_h \cdot \left(h_i \overline{\boldsymbol{B}}_{h,i} \otimes \overline{\boldsymbol{B}}_{h,i} \right),
\end{aligned} \tag{24}$$

where $h_i := z_i - z_{i-1}$.

Under the Boussinesq approximation, we assume that $\rho = \rho_0 + \widehat{\rho}$, where ρ_0 is the constant background density, and $\widehat{\rho} \ll \rho_0$. Considering a perturbation from the *magnetohydrostatic balance hypothesis* ($p^* = p_0^* + \widehat{p}^*$), where $\partial_z \widehat{p}^* = -\widehat{\rho} g$, the momentum equation (7) can be expressed as

$$\left(1 + \frac{\widehat{\rho}}{\rho_0} \right) (\partial_t \boldsymbol{v} + \boldsymbol{v} \cdot \nabla \boldsymbol{v} + f \boldsymbol{z} \times \boldsymbol{v}) = -\frac{\widehat{\rho}}{\rho_0} g \boldsymbol{z} - \nabla \frac{\widehat{p}^*}{\rho_0} + \frac{1}{\rho_0} \nabla \cdot (\boldsymbol{B} \otimes \boldsymbol{B}). \tag{25}$$

By neglecting the term $\widehat{\rho}/\rho_0$ on the left-hand side of (25) and following a similar procedure of vertical integration, the master equation

(24) simplifies to

$$\begin{aligned}\rho_0 h_i\left(\partial_t \overline{\boldsymbol{v}}_{h,i}+\overline{\boldsymbol{v}}_{h,i}\cdot\nabla_h\overline{\boldsymbol{v}}_{h,i}+f\boldsymbol{z}\times\overline{\boldsymbol{v}}_{h,i}\right)=-\nabla_h\Big(-\frac{1}{2}\overline{\widehat{\rho}}_i g h_i^2+h_i\widehat{p}^*\big|_{z_{i-1}}\Big)\\ +\nabla_h z_i\,\widehat{p}^*\big|_{z_i}-\nabla_h z_{i-1}\,\widehat{p}^*\big|_{z_{i-1}}+\nabla_h\cdot\left(h_i\overline{\boldsymbol{B}}_{h,i}\otimes\overline{\boldsymbol{B}}_{h,i}\right).\end{aligned}\tag{26}$$

For a one-layer reduction of the *master equation* (26), we consider a domain with a rigid bottom at $z_0=Z(x,y)$ and a free surface at $z_1=h(x,y,t)+Z(x,y)$, where $Z(x,y)$ represents a *magnetic topography*. At the free surface, the magnetic pressure is assumed to be constant, satisfying the boundary condition $\widehat{p}^*\big|_{z_1}=0$. To simplify the notation, we omit overbars, hats, and subscripts in the horizontal gradient operator ∇_h, and introduce the variables $\boldsymbol{v}:=\overline{\boldsymbol{v}}_h$ and $\boldsymbol{b}:=\overline{\boldsymbol{B}}_h$. We then use (22) and (26) and rescale $\boldsymbol{b}$ by $\frac{1}{\sqrt{\rho_0}}\boldsymbol{b}$ to derive the one-layer MTRSW model:

$$\partial_t\boldsymbol{v}+\boldsymbol{v}\cdot\nabla\boldsymbol{v}+f\boldsymbol{z}\times\boldsymbol{v}=-g\frac{\rho}{\rho_0}\nabla h-\frac{gh}{2}\nabla\Big(\frac{\rho}{\rho_0}\Big)-g\frac{\rho}{\rho_0}h\nabla Z+\frac{1}{h}\nabla\cdot(h\boldsymbol{b}\otimes\boldsymbol{b}),\tag{27}$$

$$\partial_t\rho+\boldsymbol{v}\cdot\nabla\rho=0,\tag{28}$$

$$\partial_t\boldsymbol{b}+\boldsymbol{v}\cdot\nabla\boldsymbol{b}=\frac{1}{h}\nabla\cdot(h\boldsymbol{v}\otimes\boldsymbol{b}),\tag{29}$$

$$\nabla\cdot(h\boldsymbol{b})=0,\quad \partial_t h+\nabla\cdot(h\boldsymbol{v})=0.\tag{30}$$

Within the framework of the MTRSW model, it is also possible to replace the rigid bottom boundary condition with a rigid lid on the uppermost material surface. For example, the set of equations (27)–(30), expressed in conservative form for atmospheric applications, can be reformulated as

$$\partial_t h+\nabla\cdot(h\boldsymbol{v})=0,\tag{31}$$

$$\partial_t(h\boldsymbol{v})+\nabla\cdot(h\boldsymbol{v}\otimes\boldsymbol{v})+fh\boldsymbol{z}\times\boldsymbol{v}=-\nabla\Big(\frac{\theta h^2}{2}\Big)-\theta h\nabla Z+\nabla\cdot(h\boldsymbol{b}\otimes\boldsymbol{b}),\tag{32}$$

$$\partial_t(h\theta)+\nabla\cdot(h\theta\boldsymbol{v})=0,\tag{33}$$

$$\partial_t(h\boldsymbol{b})+\nabla\cdot(h\boldsymbol{v}\otimes\boldsymbol{b}-h\boldsymbol{b}\otimes\boldsymbol{v})=0,\tag{34}$$

$$\nabla\cdot(h\boldsymbol{b})=0,\tag{35}$$

where $\theta=g\frac{T}{T_0}$ represents the buoyancy, T is the potential temperature, and T_0 is a reference potential temperature.

The Hall term can be incorporated within the framework of the MTRSW model to enhance its fidelity in capturing small-scale plasma dynamics. In shallow water MHD models, the inclusion of the Hall term becomes critical when ion inertial effects are non-negligible. At these scales, the conventional assumption of ions and electrons moving together as a single fluid no longer holds. Instead, the Hall term accounts for their different motion, leading to a decoupling of their dynamics. While electrons remain tightly bound to magnetic field lines, ions exhibit more independent motion. This decoupling is particularly significant in processes like magnetic reconnection, where the Hall effect enables rapid changes in magnetic topology by allowing ions and electrons to respond differently to electromagnetic forces. Additionally, the Hall term introduces modified wave dispersion and facilitates the development of small-scale magnetic structures.

The primary distinction between ideal MHD and Hall MHD lies in their treatment of small-scale phenomena and the additional physics incorporated in Hall MHD. Ideal MHD assumes the plasma behaves as a single perfectly conductive fluid, leading to the well-known *frozen-in* condition: $\boldsymbol{E}+\boldsymbol{v}\times\boldsymbol{B}=0$, where $\boldsymbol{E}$ is the electric field. This condition simplifies the induction equation to $\partial_t\boldsymbol{B}=\nabla\times(\boldsymbol{v}\times\boldsymbol{B})$, which describes large-scale, nondispersive behaviors, such as the propagation of Alfvén waves. Magnetic reconnection in this framework is slow and governed by resistivity. In contrast, Hall MHD incorporates the Hall term $\alpha_H(\boldsymbol{J}\times\boldsymbol{B})$ into the generalized Ohm's law:

$$\boldsymbol{E}+\boldsymbol{v}\times\boldsymbol{B}=\alpha_H(\boldsymbol{J}\times\boldsymbol{B}),\tag{36}$$

where α_H can be taken to be constant in the first approximation, or to be a function of the ion skin depth. Equation (36), which accounts for the decoupling of ion and electron dynamics on scales comparable to the ion inertial length, leads to the following modified induction equation:

$$\partial_t\boldsymbol{B}+(\boldsymbol{v}\cdot\nabla)\boldsymbol{B}=(\boldsymbol{B}\cdot\nabla)\boldsymbol{v}-\alpha_H\nabla\times(\boldsymbol{B}\cdot\nabla\boldsymbol{B}).\tag{37}$$

The corresponding equation for the horizontal component $\boldsymbol{b}$ of $\boldsymbol{B}$, which is to be averaged to obtain the corresponding MTRSW equations, can be written as

$$\partial_t\boldsymbol{b}+(\boldsymbol{v}\cdot\nabla)\boldsymbol{b}=(\boldsymbol{B}\cdot\nabla)\boldsymbol{v}-\alpha_H\boldsymbol{z}\times\nabla\times(\boldsymbol{B}\cdot\nabla c).\tag{38}$$

As mentioned earlier, the vertical component of the magnetic field, c, though not explicitly appearing in the MTRSW equations, is nonzero inside the fluid layer and can be computed using (16).

We then assume that $c(x,y,t)\big|_{z_0} = 0$ and rewrite the expression $\boldsymbol{B}\cdot\nabla c$ in (38) with the help of (16) used with $z_{i-1} = z_0$ as

$$\boldsymbol{B}\cdot\nabla c = c\partial_z c + \boldsymbol{b}\cdot\nabla_h c = (z-z_0)\left[(\nabla_h\cdot\boldsymbol{b})^2 - \boldsymbol{b}\cdot\nabla_h(\nabla_h\cdot\boldsymbol{b})\right]. \tag{39}$$

Vertically averaging this term (39) gives a Hall correction to the MTRSW equations. After dropping the subscript h at ∇, we obtain the Hall-MTRSW equations:

$$\partial_t h + \nabla\cdot(h\boldsymbol{v}) = 0, \tag{40}$$

$$\partial_t(h\boldsymbol{v}) + \nabla\cdot(h\boldsymbol{v}\otimes\boldsymbol{v}) + fh\boldsymbol{z}\times\boldsymbol{v} = -\nabla\left(\frac{\theta h^2}{2}\right) - \theta h\nabla Z + \nabla\cdot(h\boldsymbol{b}\otimes\boldsymbol{b}), \tag{41}$$

$$\partial_t(h\theta) + \nabla\cdot(h\theta\boldsymbol{v}) = 0, \tag{42}$$

$$\partial_t(h\boldsymbol{b}) + \nabla\cdot(h\boldsymbol{v}\otimes\boldsymbol{b} - h\boldsymbol{b}\otimes\boldsymbol{v}) + \alpha_H\frac{h^2}{2}\boldsymbol{z}\times\nabla\left[(\nabla\cdot\boldsymbol{b})^2 - \boldsymbol{b}\cdot\nabla(\nabla\cdot\boldsymbol{b})\right] = 0, \tag{43}$$

$$\nabla\cdot(h\boldsymbol{b}) = 0, \tag{44}$$

which, compared with the MTRSW equations (31)–(35), have one extra term on the RHS of (43). Recall that in (40)–(44), θ may be either $g\frac{\rho}{\rho_0}$ or $g\frac{T}{T_0}$.

To examine the impact of temperature gradients within the MTRSW framework, we consider equations (31)–(35) with a flat bottom topography ($Z\equiv 0$) and study an idealized axisymmetric localized vortex on an f-plane (with the constant Coriolis parameter $f(y)\equiv f_0$). For clarity, the equations are reformulated in polar coordinates (r,φ):

$$\partial_t h + \partial_r(h\mathtt{u}) + \frac{1}{r}\partial_\varphi(h\mathtt{v}) + \frac{1}{r}(h\mathtt{u}) = 0, \tag{45}$$

$$\frac{\mathrm{d}\mathtt{u}}{\mathrm{d}t} - \frac{\mathtt{v}^2}{r} - f\mathtt{v} = -\theta\partial_r h + \mathtt{a}\partial_r\mathtt{a} + \frac{\mathtt{b}}{r}\partial_\varphi\mathtt{a} - \frac{\mathtt{b}^2}{r} - \frac{h}{2}\partial_r\theta, \tag{46}$$

$$\frac{\mathrm{d}\mathtt{v}}{\mathrm{d}t} + \frac{\mathtt{u}\mathtt{v}}{r} + f\mathtt{u} = -\frac{\theta}{r}\partial_\varphi h + \mathtt{a}\partial_r\mathtt{b} + \frac{\mathtt{b}}{r}\partial_\varphi\mathtt{b} + \frac{\mathtt{a}\mathtt{b}}{r} - \frac{h}{2r}\partial_\varphi\theta, \tag{47}$$

$$\partial_t\theta + \mathtt{u}\partial_r\theta + \frac{\mathtt{v}}{r}\partial_\varphi\theta = 0, \tag{48}$$

$$\frac{\mathrm{d}\mathtt{a}}{\mathrm{d}t} - \mathtt{a}\partial_r\mathtt{u} - \frac{\mathtt{b}}{r}\partial_\varphi\mathtt{u} = 0, \tag{49}$$

$$\frac{\mathrm{d}\mathtt{b}}{\mathrm{d}t} - \mathtt{a}\partial_r\mathtt{v} - \frac{\mathtt{b}}{r}\partial_\varphi\mathtt{v} + \frac{1}{r}(\mathtt{a}\mathtt{v} - \mathtt{b}\mathtt{u}) = 0, \tag{50}$$

$$\partial_r(h\mathtt{a}) + \frac{1}{r}\partial_\varphi(h\mathtt{b}) + \frac{1}{r}(h\mathtt{a}) = 0, \tag{51}$$

where the velocity and magnetic fields are expressed in the polar coordinates as $\boldsymbol{u} = \mathtt{u}\widehat{\boldsymbol{r}} + \mathtt{v}\widehat{\boldsymbol{\varphi}}$ and $\mathscr{B} = \mathtt{a}\widehat{\boldsymbol{r}} + \mathtt{b}\widehat{\boldsymbol{\varphi}}$, where $\widehat{\boldsymbol{r}}$ and $\widehat{\boldsymbol{\varphi}}$ are unit vectors in the r and φ directions, respectively, and the material derivative is defined as $\frac{\mathrm{d}}{\mathrm{d}t} := \partial_t + \mathtt{u}\partial_r + \frac{\mathtt{v}}{r}\partial_\varphi$. The axisymmetric *thermo-magneto-cyclo-geostrophic (TMCG) balanced state* for the background fields $h = H(r)$, $\mathtt{u}\equiv 0$, $\mathtt{v} = V(r)$, $\theta = \Theta(r)$, $\mathtt{a}\equiv 0$, and $\mathtt{b} = \mathscr{B}(r)$ is given by

$$\frac{V^2}{r} + fV = \Theta\partial_r H + \frac{\mathscr{B}^2}{r} + \frac{H}{2}\partial_r\Theta. \tag{52}$$

Equation (52) extends the classical thermal wind balance to include magnetic tension effects. This balance condition describes the equilibrium between centrifugal forces (V^2/r), Coriolis forces (fV), buoyancy gradients ($\Theta\partial_r H + \frac{H}{2}\partial_r\Theta$), and magnetic tension ($\mathscr{B}^2/r$). By introducing small perturbations about the state of rest (52), equations (45)–(51) are linearized, and their normal-mode solutions are sought with harmonic dependence on time and azimuthal angle:

$$(h',\mathtt{u}',\mathtt{v}',\theta',\mathtt{a}',\mathtt{b}')(r,\varphi,t) = \mathrm{Re}\left[(\widetilde{h}(r), i\widetilde{\mathtt{u}}(r), \widetilde{\mathtt{v}}(r), \widetilde{\theta}(r), i\widetilde{\mathtt{a}}(r), \widetilde{\mathtt{b}}(r))e^{i(\ell\varphi-\omega t)}\right], \tag{53}$$

where ℓ is the azimuthal wavenumber, and $\omega = \omega_R + i\omega_I$ is the complex eigenfrequency. A positive imaginary part of ω_I indicates instability with a linear growth rate. By using the Rossby deformation radius R_d as the scale for r, f_0^{-1} as the scale for t, and $\sqrt{\Theta_0 H_0}$ as the scale for the velocity, we obtain that ω is an eigenvalue satisfying

$$\begin{pmatrix} \boldsymbol{A}_{11} & \boldsymbol{A}_{12} \\ \boldsymbol{A}_{21} & \boldsymbol{A}_{22} \end{pmatrix} \begin{pmatrix} \widetilde{\boldsymbol{x}}_1 \\ \widetilde{\boldsymbol{x}}_2 \end{pmatrix} = \omega \begin{pmatrix} \widetilde{\boldsymbol{x}}_1 \\ \widetilde{\boldsymbol{x}}_2 \end{pmatrix}, \tag{54}$$

where $\boldsymbol{A}_{ij}$ are 3×3 submatrices of the original system:

$$\boldsymbol{A}_{11} = \begin{pmatrix} \frac{\ell V^*}{r^*} & H^* D_{r^*} + \frac{1}{r^*} D_{r^*}(r^* H^*) & \frac{\ell H^*}{r^*} \\ -\Theta^* D_{r^*} - \frac{1}{2} D_{r^*}\Theta^* & \frac{\ell V^*}{r^*} & f^* + \frac{2V^*}{r^*} \\ \frac{\ell \Theta^*}{r^*} & f^* + \frac{V^*}{r^*} + D_{r^*} V^* & \frac{\ell V^*}{r^*} \end{pmatrix}, \tag{55}$$

$$\boldsymbol{A}_{12} = \begin{pmatrix} 0 & 0 & 0 \\ -D_{r^*} H^* - \frac{H^*}{2} D_{r^*} & -\frac{\ell \mathscr{B}^*}{r^*} & -\frac{2\mathscr{B}^*}{r^*} \\ \frac{\ell H^*}{2r^*} & -D_{r^*}\mathscr{B}^* - \frac{\mathscr{B}^*}{r^*} & -\frac{\ell \mathscr{B}^*}{r^*} \end{pmatrix}, \tag{56}$$

$$\boldsymbol{A}_{21} = \begin{pmatrix} 0 & D_{r^*}\Theta^* & 0 \\ 0 & -\frac{\ell \mathscr{B}^*}{r^*} & 0 \\ 0 & D_{r^*}\mathscr{B}^* - \frac{\mathscr{B}^*}{r^*} & -\frac{\ell \mathscr{B}^*}{r^*} \end{pmatrix}, \quad \boldsymbol{A}_{22} = \begin{pmatrix} \frac{\ell V^*}{r^*} & 0 & 0 \\ 0 & \frac{\ell V^*}{r^*} & 0 \\ 0 & \frac{V^*}{r^*} - D_{r^*} V^* & \frac{\ell V^*}{r^*} \end{pmatrix}, \tag{57}$$

$\widetilde{\boldsymbol{x}}_1 = (\widetilde{h}, \widetilde{\mathtt{u}}, \widetilde{\mathtt{v}})^\top$, and $\widetilde{\boldsymbol{x}}_2 = (\widetilde{\theta}, \widetilde{\mathtt{a}}, \widetilde{\mathtt{b}})^\top$. Here, some of the variables are marked with an asterisk to stress their non-dimensional nature, and D_{r^*} denotes differentiation with respect to r^*. For the linear stability analysis of this eigenproblem, a pseudospectral collocation method is used: The system is discretized over Chebyshev collocation points with D_{r^*} replaced by the Chebyshev differentiation operator. The transformed Chebyshev grid maps standard Chebyshev points to a semi-infinite domain $[0,\infty)$, concentrating resolution near the origin where sharp gradients or boundary layers often occur.

We construct a background TMCG balance state consistent with (52) by setting $H(r) = 1$ and using a zonal velocity profile given by [9]

$$V(r) = \gamma (r - r_0)^\alpha e^{-m(r-r_0)^\beta}, \quad \alpha, \beta, \gamma, m \geq 0, \tag{58}$$

where γ determines the intensity of the velocity field, r_0 specifies the distance of the velocity peak of the vortex from the center, and other parameters shape the velocity distribution. We assume that the potential temperature, $\Theta(r)$, is proportional to the warm core of a pressure anomaly in geostrophic balance. Its non-dimensional form is expressed as $\Theta(r) = 1 - \delta[F(r) - 1]$, where $F(r) = \int_r^\infty \left(f_0 + \frac{V(r')}{r'}\right) V(r')\, \mathrm{d}r'$. We then use (52) to determine the magnetic field profile:

$$\mathscr{B}(r) = \sqrt{V^2(r) + r f_0 V(r) - \frac{r}{2}\Theta'(r) H(r)}. \tag{59}$$

We set the following parameter values: $\gamma = 0.4$, $\alpha = 4$, $\beta = 0.45$, $m = 14$, $r_0 = 0.1$, and $f_0 = 1$, and take 400 Chebyshev collocation points. Finally, we consider two scenarios: one with a trivial background temperature anomaly ($\delta = 0.001$) and the other with a nontrivial temperature anomaly ($\delta = 1$); see Fig. 1. The corresponding unstable mode with an azimuthal wavenumber $\ell = 2$ for these configurations is shown in Fig. 2. Then, the initial data can be obtained as follows:

$$\begin{aligned} &h(x,y,0) = H(r) + \varepsilon h', \quad u(x,y,0) = -V(r)\sin\varphi + \varepsilon \mathtt{u}', \quad v(x,y,0) = V(r)\cos\varphi + \varepsilon \mathtt{v}', \\ &\theta(x,y,0) = \Theta(r) + \varepsilon \theta', \quad a(x,y,0) = -\mathscr{B}(r)\sin\varphi + \varepsilon \mathtt{a}', \quad b(x,y,0) = \mathscr{B}(r)\cos\varphi + \varepsilon \mathtt{b}', \end{aligned} \tag{60}$$

where ε is a perturbation coefficient, which is taken as 0.02 in this work.

The numerical method employed in this study is a second-order path-conservative central-upwind scheme, utilizing flux globalization for solving the MTRSW equations [1]. A comparison of the evolution of instabilities in these two scenarios reveals that a nontrivial potential temperature significantly enhances the growth of instabilities, allowing satellite magnetic vortices to persist for longer periods; see Fig. 3.

In this study, we introduced the *Magnetohydrodynamic Thermal Rotating Shallow Water (MTRSW) model*, which integrates thermal dynamics and magnetohydrodynamic (MHD) principles into the traditional shallow water framework. This novel model captures the interplay between temperature gradients, magnetic field evolution, and rotational effects, providing a tool for investigating magnetized geophysical and astrophysical systems. Our findings reveal that nontrivial potential temperature gradients play a pivotal role in stability of magnetic structures, with numerical simulations showing the emergence of more persistent magnetic vortices compared

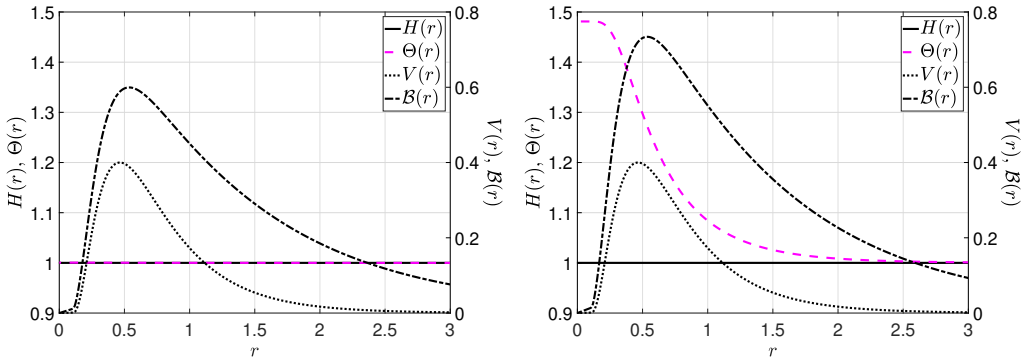

FIG. 1. Radial profiles of axisymmetric variables in the TMCG balanced state for trivial (left panel) and nontrivial (right panel) background potential temperature anomalies.

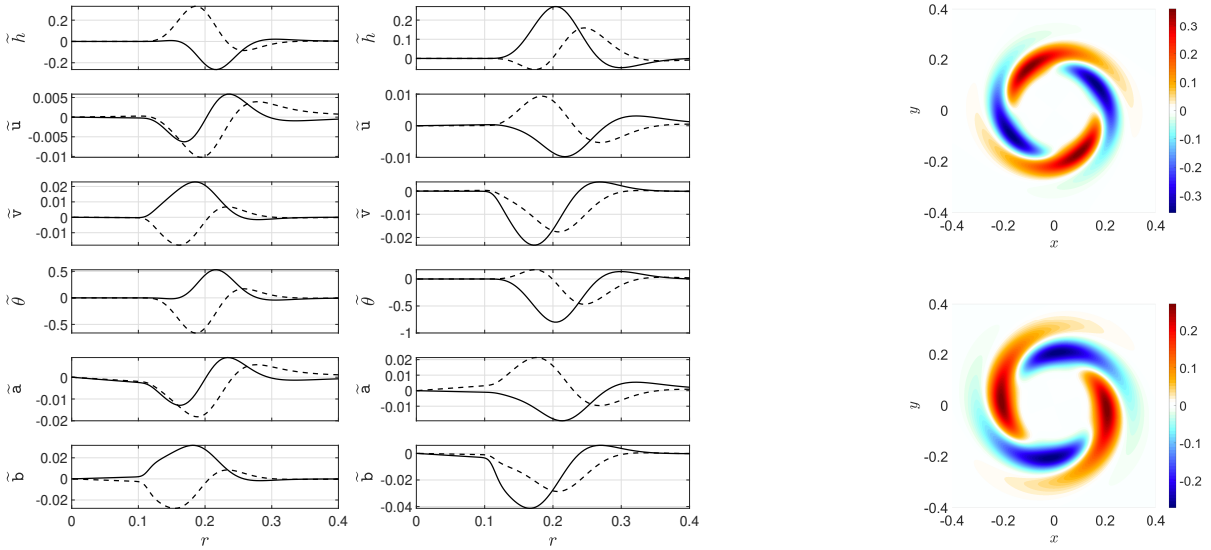

FIG. 2. Results from linear stability analysis of the thermo-magneto-cyclo-geostrophic (TMCG) base state. The left and middle columns show the radial structure of the unstable eigenmode with azimuthal wavenumber $\ell = 2$, including perturbations in layer thickness, radial and tangential velocity components, and magnetic field. Solid lines denote the real parts and dashed lines the imaginary parts of the eigenfunctions. The left panel corresponds to a trivial background potential temperature anomaly, while the middle panel reflects a nontrivial anomaly. The right column displays the spatial structure of the eigenfunction $\widetilde{h}$ in the (x,y)-plane for the trivial (top) and nontrivial (bottom) thermal background cases.

to systems with trivial thermal profiles. This result highlights the critical influence of thermal variations in modulating the stability and morphology of magnetic fields under rotating conditions. Furthermore, the incorporation of the Hall term in the MTRSW model provides new insights into the mechanisms driving fast magnetic reconnection, a phenomenon essential for energy dissipation in magnetized flows. This term also captures the influence of distinct small-scale structures, enhancing the realism of simulations and bridging the gap between theoretical predictions and observed magnetic behaviors.

While the current MTRSW formulation captures essential physics of rotating, stratified magnetofluids, several idealizations warrant consideration. The inviscid assumption, while mathematically convenient for isolating conservative dynamics, precludes treatment of dissipative processes in turbulent regimes. Similarly, the two-dimensional geometry, though appropriate for large-scale dynamics, filters out potentially important three-dimensional effects such as vortex stretching and secondary instabilities. These simplifications enable tractable analysis of fundamental processes but limit direct application to highly turbulent natural systems like solar tachoclines or planetary magnetospheres.

Acknowledgment: The work of Y. Cao was supported in part by the Guangdong Basic and Applied Basic Research Foundation (No. 2025A1515012249), the Tianyuan Fund for Mathematics of NSFC (No. 12526601) and Shenzhen Science and Technology Program (No. JCYJ20250604173044021). A. Kurganov was supported in part by NSFC grants 12171226 and W2431004. C. Wang

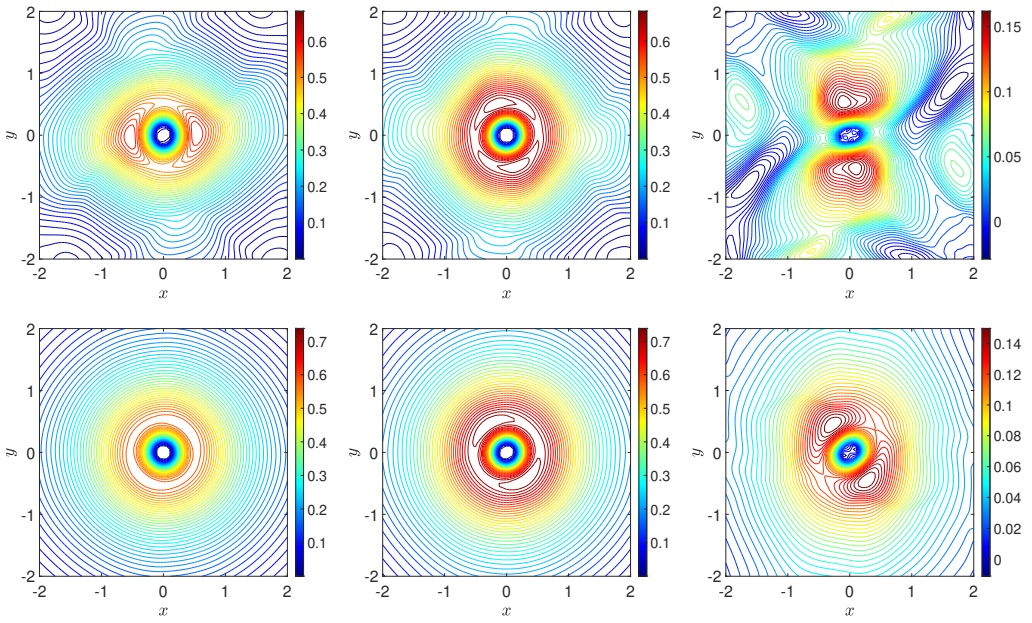

FIG. 3. **Upper row**: Magnetic field of the unstable mode with azimuthal wavenumber $\ell = 2$ in the (x,y)-plane for a trivial (left panel) and nontrivial (middle panel) background potential temperature gradient at time $t = 50[f_0^{-1}]$. The right panel shows the difference between these two scenarios. **Lower row**: Same as the upper row, but at time $t = 200[f_0^{-1}]$.

was supported in part by NSFC grant 12401524 and the China Postdoctoral Science Foundation (No. 2024M761273).

[1] Y. Cao, A. Kurganov, M. Rostami, C. Wang, and V. Zeitlin. Locally divergence-free well-balanced path-conservative central-upwind schemes for thermal magnetic rotating shallow water equations. *Submitted; preprint available at https://sites.google.com/view/alexander-kurganov/publications*, 2025.

[2] P. A. Gilman. Magnetohydrodynamic "shallow water" equations for the solar tachocline. *Astrophys. J. Lett.*, 544(1):L79, nov 2000. doi:10.1086/317291. URL https://dx.doi.org/10.1086/317291.

[3] D. D. Holm, E. Luesink, and P. Wei. Stochastic mesoscale circulation dynamics in the thermal ocean. *Phys. Fluids*, 33(4):046603, 2021. ISSN 1070-6631. doi:10.1063/5.0040026. URL https://doi.org/10.1063/5.0040026.

[4] A. Kurganov, Y. Liu, and V. Zeitlin. Moist-convective thermal rotating shallow water model. *Phys. Fluids*, 32(6):066601, 2020. ISSN 1070-6631. doi:10.1063/5.0007757. URL https://doi.org/10.1063/5.0007757.

[5] A. Kurganov, Y. Liu, and V. Zeitlin. Interaction of tropical cyclone-like vortices with sea-surface temperature anomalies and topography in a simple shallow-water atmospheric model. *Phys. Fluids*, 33(10):106606, 2021.

[6] R. L. Lavoie. A mesoscale numerical model of lake-effect storms. *J. Atmos. Sci.J. Atmos. Sci.*, 29(6):1025–1040, 1972. doi:10.1175/1520-0469(1972)029¡1025:AMNMOL¿2.0.CO;2. URL https://journals.ametsoc.org/view/journals/atsc/29/6/1520-0469_1972_029_1025_amnmol_2_0_co_2.xml.

[7] P. Ripa. Conservation laws for primitive equations models with inhomogeneous layers. *Geophys. Astrophys. Fluid Dyn.*, 70(1-4):85–111, 1993. doi:10.1080/03091929308203588. URL https://doi.org/10.1080/03091929308203588.

[8] P. Ripa. Low frequency approximation of a vertically averaged ocean model with thermodynamics. *Rev. Mex. Fís.*, 42(1):117–135, 1996.

[9] M. Rostami and V. Zeitlin. An improved moist-convective rotating shallow-water model and its application to instabilities of hurricane-like vortices. *Q. J. R. Meteorol. Soc.*, 144(714):1450–1462, 2018. doi:https://doi.org/10.1002/qj.3292. URL https://rmets.onlinelibrary.wiley.com/doi/abs/10.1002/qj.3292.

[10] M. Rostami, B. Zhao, and S. Petri. On the genesis and dynamics of Madden–Julian oscillation-like structure formed by equatorial adjustment of localized heating. *Q. J. R. Meteorol. Soc.*, 148(749):3788–3813, 2022. doi:https://doi.org/10.1002/qj.4388. URL https://rmets.onlinelibrary.wiley.com/doi/abs/10.1002/qj.4388.

[11] M. Rostami, S. Petri, B. Fallah, and F. Fazel-Rastgar. Aeolus 2.0's thermal rotating shallow water model: A new paradigm for simulating extreme heatwaves, westerly jet intensification, and more. *Phys. Fluids.*, 37(1):016604, 2025. ISSN 1070-6631. doi:10.1063/5.0244908. URL https://doi.org/10.1063/5.0244908.

[12] M. L. Salby. Deep circulations under simple classes of stratification. *Tellus*, 41(1):48–65, 1989. doi:10.3402/tellusa.v41i1.11820. URL https://doi.org/10.3402/tellusa.v41i1.11820.